Carcinogenesis, 2018, Vol. 39, No. 2, 232–241

doi:10.1093/carcin/bgx135
Advance Access publication November 29, 2017
Original Article

ORIGINAL ARTICLE

Identification of more than 100 structurally unique DNA-phosphate adducts formed during rat lung carcinogenesis by the tobacco-specific nitrosamine 4-(methylnitrosamino)-1-(3-pyridyl)-1-butanone

Bin Ma*, Adam T. Zarth, Erik S. Carlson, Peter W.Villalta, Pramod Upadhyaya, Irina Stepanov and Stephen S. Hecht

Masonic Cancer Center, University of Minnesota, Minneapolis, MN 55455, USA

*To whom correspondence should be addressed. Tel: +1 612 625 4925; Fax: +1 612 624 3869; Email: bma@umn.edu

Abstract

The tobacco-specific nitrosamine 4-(methylnitrosamino)-1-(3-pyridyl)-1-butanone (NNK) is a powerful lung carcinogen in animal models and is considered a causative factor for lung cancer in people who use tobacco products. NNK undergoes metabolic activation—a critical step in its mechanism of carcinogenesis—to an intermediate which reacts with DNA to form pyridyloxobutyl DNA base and phosphate adducts. Another important metabolic pathway of NNK is its conversion to 4-(methylnitrosamino)-1-(3-pyridyl)-1-butanol (NNAL), which similarly forms pyridylhydroxybutyl DNA base adducts that have been characterized previously. In this study, we investigated the potential formation of pyridylhydroxybutyl DNA phosphate adducts. We report the characterization and quantitation of 107 structurally unique pyridylhydroxybutyl DNA phosphate adducts in the lungs of rats treated chronically with a carcinogenic dose of 5 ppm of NNK in their drinking water for up to 70 weeks, by using a novel liquid chromatography-nanoelectrospray ionization-high-resolution tandem mass spectrometry method. Our findings demonstrate that pyridylhydroxybutyl phosphate adducts account for 38–55 and 34–40% of all the measured pyridine-containing DNA adducts in rat lung and liver, respectively, upon treatment with NNK. Some of the pyridylhydroxybutyl DNA phosphate adducts persisted in both tissues for over 70 weeks, suggesting that they could be potential biomarkers of chronic exposure to NNK and NNAL. This study provides comprehensive characterization and relative quantitation of a panel of NNK/NNAL-derived DNA phosphate adducts, thus identifying NNK as the source of the most structurally diverse set of DNA adducts identified to date from any carcinogen.

Introduction

All tobacco products contain 4-(methylnitrosamino)-1-(3-pyridyl)-1-butanone (NNK), a tobacco-specific nitrosamine which is a powerful pulmonary carcinogen in rats, mice and hamsters, inducing mainly adenocarcinoma, independent of its route of administration (1–4). For example, in one recent study, F-344 rats were treated with NNK in the drinking water (5 ppm) for up to 90 weeks (5). All treated rats had histologically confirmed lung tumors, most of which were classified as carcinoma; metastases to the pancreas were also observed. In rodents and humans, NNK is extensively metabolized to 4-(methylnitrosamino)-1-(3-pyridyl)-1-butanol (NNAL) which is also a potent and selective pulmonary carcinogen with activity similar to that of NNK (4,5). All humans who use tobacco products—either cigarettes or smokeless tobacco—have NNAL in their urine (6–11). NNK is considered as one likely cause of lung cancer—particularly adenocarcinoma of the lung—in cigarette smokers (3,12). Consistent with its organospecificity for the lung, a recent epidemiologic study has also demonstrated

Received: August 3, 2017; **Revised:** October 25, 2017; **Accepted:** November 25, 2017

Abbreviations

HCD	higher-energy collisional dissociation
LC	liquid chromatography
NNK	4-(methylnitrosamino)-1-(3-pyridyl)-1-butanone
NNAL	4-(methylnitrosamino)-1-(3-pyridyl)-1-butanol
NSI	nanoelectrospray ionization

a significantly elevated risk of lung cancer in non-smokers who were exclusive users of oral smokeless tobacco products (chewing tobacco and snuff), which have a less complex mixture of carcinogens than cigarette smoke, and in which NNK is one of the most abundant strong carcinogens (13). NNK and the related carcinogen *N*′-nitrosonornicotine are considered 'carcinogenic to humans' by the International Agency for Research on Cancer (1).

A critical step in carcinogenesis by nitrosamines such as NNK and NNAL is formation of DNA adducts, which can cause miscoding and permanent mutations in growth control genes such as *K-RAS* (14,15). Identification of the relevant DNA adducts can significantly enhance our understanding of mechanisms of cancer induction, potentially leading to biomarkers for the identification of particularly susceptible users of tobacco products and providing insights for cancer prevention.

Metabolic activation of NNK to intermediates that react with DNA to form adducts occurs by α-hydroxylation, a cytochrome P450-catalyzed pathway that is typical for nitrosamines (4,16). α-Hydroxylation of both the methylene and methyl carbons is observed; only the latter is considered here. As shown in Figure 1, α-hydroxylation of the NNK methyl group produces the unstable intermediate α-hydroxymethylNNK (**4**) which spontaneously loses formaldehyde to produce diazohydroxide **6**. This intermediate can further decompose to diazonium ion **8**, which is highly electrophilic and reacts with DNA to produce pyridyloxobutyl (POB)-base adducts such as 7-[4-(3-pyridyl)-4-oxobutyl]Gua (7-POB-Gua), O^6-POB-dGuo and O^2-POB-dThd, as well as phosphate adducts such as $B_1p(POB)B_2$, which have been previously characterized (and were referred to as B_1popB_2) (5,17–21). The NNK metabolite NNAL (**2**) also undergoes α-hydroxylation to similarly produce diazonium ion **9** (4,22). Diazonium ion **9** reacts with DNA bases to form 4-[(3-pyridyl)-4-hydroxybutyl] (PHB)-base adducts which have been previously characterized (23,24), but also has the potential to form phosphate adducts in DNA such as $B_1p(PHB)_sB_2$, where PHB represents pyridylhydroxybutyl and the subscript s represents 'straight chain' (Figure 1). Diazonium ion **9** further rearranges to carbocation **10** (22), which can also form adducts with both DNA bases and phosphate [e,g., $B_1p(PHB)_bB_2$, where the subscript b represents 'branched']. Thus, DNA phosphate adducts of NNAL arising through intermediates **9** and **10**, and collectively called $B_1p(PHB)B_2$, have not been previously investigated and are the subject of this report.

We developed a novel liquid chromatography (LC)-nanoelectrospray ionization (NSI)-high-resolution tandem mass spectrometry (HRMS/MS) method for analysis of the potentially complex array of DNA phosphate adducts formed in the NNAL pathway of NNK metabolism. DNA phosphate adducts from this pathway were characterized in reactions of NNALOAc (**3**), a stable precursor to intermediate **5** formed in NNAL metabolism, with DNA, and in lung and liver DNA of rats treated with 5 ppm of NNK in the drinking water for 10, 30, 50 and 70 weeks, conditions which cause lung tumors in all animals as noted above.

Materials and methods

Materials and chemicals

Two diastereomers of dCp[4-oxo-4-(3-pyridyl)butyl]dC [Cp(POB)C-1 and Cp(POB)C-2] (21), and two diastereomers of Tp[4-oxo-4-(3-pyridyl)butyl]T [Tp(POB)T-1 and Tp(POB)T-2] were procured from WuXi AppTec (Hong Kong). The structures of Tp(POB)T-1 and Tp(POB)T-2 were confirmed by one-dimensional and two-dimensional NMR in our laboratory (Supplementary Figure 1, available at *Carcinogenesis* Online). NNALOAc was synthesized based on our previously published method (22). 5′-Dimethoxytrityl [$^{13}C_{10}{}^{15}N_2$]2′-thymidine-3′-[(2-cyanoethyl)-(*N*,*N*-diisopropyl)]phosphoramidite was obtained from Cambridge Isotope Laboratories (Tewksbury, MA). All other nucleoside phosphoramidites, solvents and solid supports required for the solid phase synthesis of dinucleotide [$^{13}C_{10}{}^{15}N_2$]2′-TpT were acquired from Glen Research Corp. (Sterling, VA). Enzymes and reagents for DNA isolation were purchased from Qiagen Sciences (Germantown, MD). All other chemicals and solvents were obtained from Sigma-Aldrich Chemical Co. (Milwaukee, WI).

Synthesis of chemical standards

Cp(PHB)$_s$C and Tp(PHB)$_s$T

dCp[4-Hydroxy-4-(3-pyridyl)butyl]dC [Cp(PHB)$_s$C] isomers were synthesized by treating Cp(POB)C-1 or Cp(POB)C-2 with sodium borohydride in H_2O at room temperature for 60 min. A single peak was detected in each reaction solution by LC-MS in the full scan mode, and the presence of Cp(PHB)$_s$C was confirmed by MS fragmentation data (Supplementary Figure 2, available at *Carcinogenesis* Online). Two isomers, Cp(PHB)$_s$C-1 [from Cp(POB)C-1] and Cp(PHB)$_s$C-2 [from Cp(POB)C-2], were identified. Similarly, Tp[4-hydroxy-4-(3-pyridyl)butyl]T [Tp(PHB)$_s$T] isomers were synthesized by treating Tp(POB)T-1 or Tp(POB)T-2 with sodium borohydride in H_2O at room temperature for 60 min. A single peak was detected in each reaction solution by LC-MS in the full scan mode, and the presence of Tp(PHB)$_s$T was confirmed by MS fragmentation data (Supplementary Figure 3, available at *Carcinogenesis* Online). Two isomers, Tp(PHB)$_s$T-1 [from Tp(POB)T-1] and Tp(PHB)$_s$T-2 [from Tp(POB)T-2], were identified. The isomers of Cp(PHB)$_s$C and Tp(PHB)$_s$T were further purified on 30 mg Strata-X cartridges (Phenomenex), and their structures were confirmed by one-dimensional and two-dimensional NMR (Supplementary Figures 4 and 5, available at *Carcinogenesis* Online).

[$^{15}N_3$]Cp(PHB)$_s$C and [$^{13}C_{10}{}^{15}N_2$]Tp(PHB)$_s$T

A similar synthetic procedure to that used for the preparation of Cp(PHB)$_s$C from Cp(POB)C was used to synthesize [$^{15}N_3$]Cp(PHB)$_s$C from [$^{15}N_3$]Cp(POB)C, which was obtained in our previous study (21). The identities of [$^{15}N_3$]Cp(PHB)$_s$C-1 and [$^{15}N_3$]Cp(PHB)$_s$C-2 were confirmed via LC-MS by comparison with the corresponding unlabeled Cp(PHB)$_s$C standards. To synthesize [$^{13}C_{10}{}^{15}N_2$]Tp(PHB)$_s$T, [$^{13}C_{10}{}^{15}N_2$]2′-TpT was first prepared on a DNA synthesizer (ABI 394, Applied Biosystems, Foster City, CA) in accordance with standard solid phase oligodeoxynucleotide synthesis protocols. In this study, 5′-dimethoxytrityl[$^{13}C_{10}{}^{15}N_2$]2′-thymidine-3′-[(2-cyanoethyl)-(*N*,*N*-diisopropyl)]phosphoramidite was manually coupled to an Ac-dT-CPG solid support, followed by standard deprotection techniques performed on the DNA synthesizer (Supplementary Figure 6, available at *Carcinogenesis* Online). [$^{13}C_{10}{}^{15}N_2$]Tp(POB)T was subsequently synthesized by reacting [$^{13}C_{10}{}^{15}N_2$]2′-TpT with NNKOAc in 0.01 M NaOH (37°C) for 16 h and purified by reversed phase HPLC using a Waters 510 HPLC system. [$^{13}C_{10}{}^{15}N_2$]Tp(PHB)$_s$T was then synthesized by treating [$^{13}C_{10}{}^{15}N_2$]Tp(POB)T with sodium borohydride in H_2O at room temperature for 60 min, and purified by 30 mg Strata-X cartridges. The identity of [$^{13}C_{10}{}^{15}N_2$]Tp(PHB)$_s$T was confirmed via LC-MS by comparison with the corresponding unlabeled Tp(PHB)$_s$T standard.

In vitro and *in vivo* DNA samples

In the *in vitro* study, CT-DNA (2 mg) was incubated with NNALOAc (10 mg) in the presence of porcine liver esterase (4 units) in 0.1 M phosphate buffer (1 ml, pH 7.0) at 37°C for 12 h. NNALOAc is a chemically activated form of NNAL, which in the presence of esterase forms the same reactive intermediate **5** as produced in metabolism of NNAL by P450s (Figure 1) (22). The incubation mixture was then washed three times with 4 ml of a $CHCl_3$/

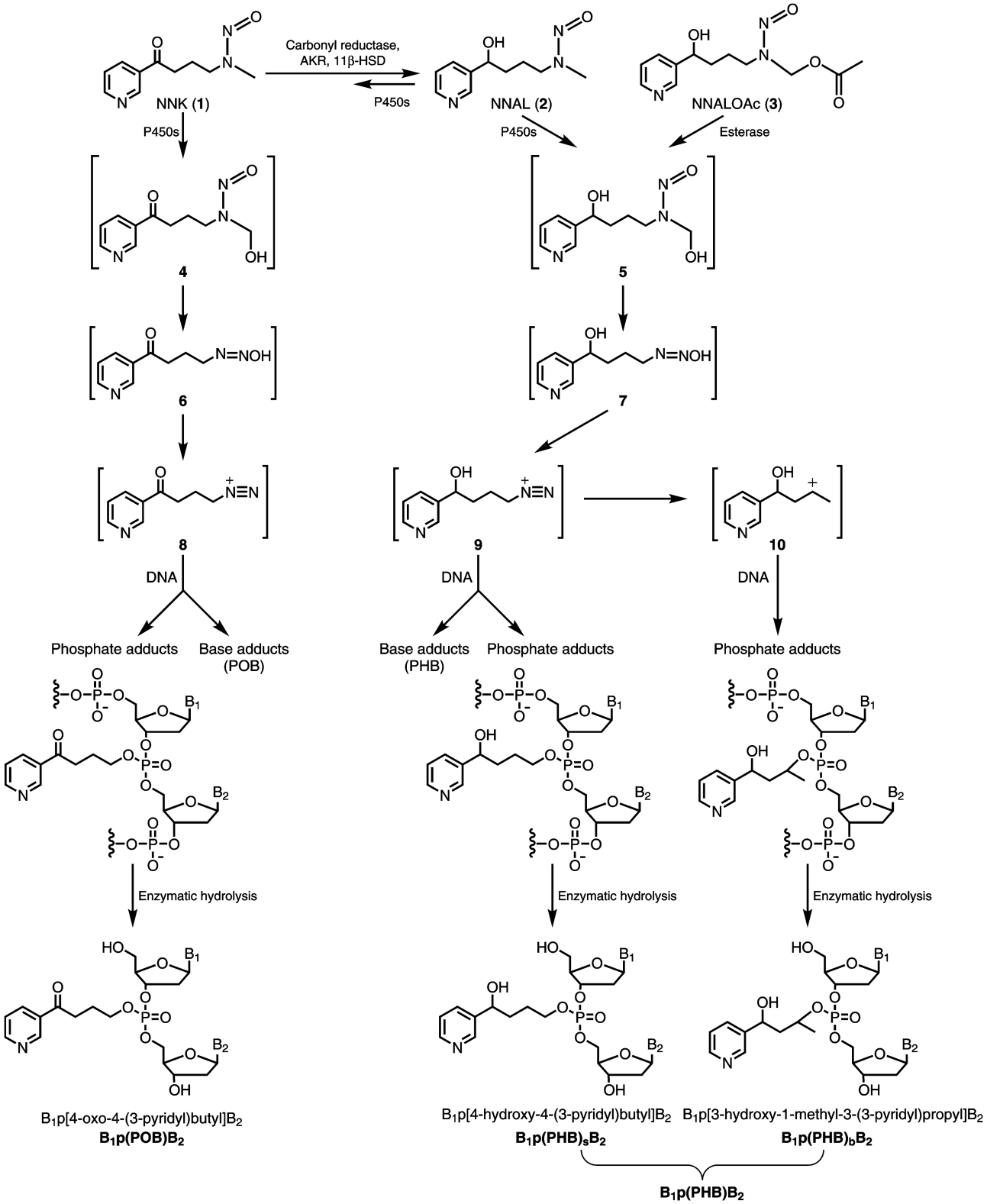

Figure 1. Pyridyloxobutyl and pyridylhydroxybutyl DNA adduct formation by NNK and NNALOAc. B_1 and B_2 represent the same or different nucleobases.

isoamyl alcohol mixture (24:1). The treated CT-DNA was precipitated via the addition of cold 2-propanol, washed with 70% EtOH and 100% EtOH sequentially, dried under a stream of N_2 and stored at –20°C until analysis. The *in vivo* DNA samples were from lung and liver tissues of male F-344 rats (n = 5 at each time points) treated chronically with 5 ppm of NNK in drinking water for 10, 30, 50 and 70 weeks, as described previously (5). DNA was isolated using our previously developed protocol (20), and stored at –20°C until analysis.

DNA hydrolysis and sample preparation

The DNA samples were dissolved in 0.6 ml of 10 mM sodium succinate buffer (pH 7.4) containing 5 mM $CaCl_2$ and 10 fmol $[^{15}N_3]$Cp(PHB)$_s$C and $[^{13}C_{10}{}^{15}N_2]$Tp(PHB)$_s$T as internal standards. The solution was then mixed with deoxyribonuclease I (60 units), phosphodiesterase I (0.03 units) and alkaline phosphatase (40 units), followed by overnight incubation at 37°C. On the next day, 20 µl of hydrolysate was collected for dGuo analysis and DNA quantitation (20). The remaining hydrolysate was filtered through 10 K centrifugal filters (Ultracel YM-10, Millipore), and the filtrates were loaded on 30-mg Strata X cartridges (Phenomenex) activated with 2 ml of MeOH and 2 ml of H_2O. The cartridges were washed with 2 ml of H_2O and 1 ml of 10% MeOH sequentially and finally eluted with 2 ml of 50% MeOH. The 50% MeOH fraction containing analytes was concentrated to dryness in a centrifugal evaporator. The residue was re-dissolved in 10 µl of deionized H_2O prior to analysis by LC-NSI-HRMS/MS.

LC-NSI-HRMS/MS analysis

The analysis was performed on an Orbitrap Fusion Tribrid mass spectrometer (Thermo Scientific, Waltham, MA) with full scan, selected-ion monitoring (SIM) and product ion scan analysis using Orbitrap detection with internal calibration using the EASY-IC feature of the Fusion instrument. A nanoLC column (75 µm i.d., 360 µm o.d., 17 cm length and 15 µm orifice) packed with Luna C_{18} bonded separation media (Phenomenex, Torrance, CA) was used. The mobile phase consisted of 5 mM NH_4OAc and CH_3CN. A 5 µl injection loop was used, and the sample (4 µl) was loaded onto the capillary column with a 900 nl/min flow rate under the initial conditions for 6.5 min at which point the injection valve position was switched to take the injection loop out of the flow path and the flow rate was reduced to 300 nl/min. Separation on the column was performed using a linear gradient with increasing CH_3CN from 2 to 18% over 24 min, followed by ramping to 90% CH_3CN within 2 min and holding at this composition for an additional 3 min. The gradient was then returned to 2% CH_3CN in 1 min, and the system was re-equilibrated at this mobile phase composition for 6 min at 900 nl/min before the next injection. The spray voltage of the mass spectrometer was 2.2 kV. The capillary temperature was 300°C, and the S-Lens RF Level was 60%. A multiplexed SIM analysis was performed whereby each ion mass of interest is sequentially isolated by the quadrupole and stored in the ion routing multipole, and upon collection of all masses of interest, all ions are transported into the Orbitrap for analysis. The $[M + H]^+$ ions of all possible phosphate adducts listed in Table 1 were analyzed in this fashion using an isolation window of 3 *m/z*, Automatic Gain Control (AGC) target of 50 000, maximum inject time of 100 ms and a resolution of 60 000. The product ion scan was performed using higher-energy collisional dissociation (HCD) fragmentation with a normalized collision energy of 25 units, isolation widths of 1 Da for all the precursor ions and product ion analysis performed with a mass range of *m/z* 100–800 at a resolution of 15 000. The accurate mass tolerance used for extraction of precursor and fragment ion signals was 5 ppm.

The quantitative analysis of Cp(PHB)$_s$C and Tp(PHB)$_s$T was performed using accurate mass extracted ion chromatograms of the product ion scan data of *m/z* 328.0945 $[C_{14}H_{19}NO_6P]^+$ for Cp(PHB)$_s$C (parent ion *m/z* 666.2), $[^{15}N_3]$Cp(PHB)$_s$C (parent ion *m/z* 669.2), Tp(PHB)$_s$T (parent ion *m/z* 696.2) and $[^{13}C_{10}{}^{15}N_2]$Tp(PHB)$_s$T (parent ion *m/z* 708.2) with a mass tolerance of 5 ppm. Quantitation was based on the peak area ratio of Cp(PHB)$_s$C or T(PHB)$_s$T to their corresponding isotope-labeled internal standards, the constructed calibration curves and the amount of internal standards added. Calibration curves were constructed for both Cp(PHB)$_s$C and Tp(PHB)$_s$T before each analysis using a series of standard solutions of Cp(PHB)$_s$C/$[^{15}N_3]$Cp(PHB)$_s$C and Tp(PHB)$_s$T/$[^{13}C_{10}{}^{15}N_2]$Tp(PHB)$_s$T. The calibration standard solutions contained a constant amount of $[^{15}N_3]$Cp(PHB)$_s$C and $[^{13}C_{10}{}^{15}N_2]$Tp(PHB)$_s$T (5 fmol on-column) and varying amounts of Cp(PHB)$_s$C and Tp(PHB)$_s$T (0.03, 0.06, 0.15, 0.3, 0.6, 3 and 15 fmol on-column). A semi-quantitative approach was applied to estimate the levels of all other phosphate adducts based on their MS signal intensities compared to Cp(PHB)$_s$C or Tp(PHB)$_s$T under the SIM scan mode. Doubly charged peaks ($[M + 2H]^{2+}$, Table 1), except for the T–T nucleobase combination, were observed during sample analysis (Supplementary Figure 7, available at *Carcinogenesis* Online), and their contribution to signal intensity was added when estimating the levels of these adducts. The average signal response of the Cp(PHB)$_s$C and Tp(PHB)$_s$T calibration curves was used to estimate the levels of other phosphate adducts.

All data are presented as mean ± standard deviation (SD). Comparison of adduct levels at different time points were performed using analysis of variance (ANOVA) with Bonferroni correction for multiple comparisons. A *P* value less than 0.05 was considered significant.

Results

Characterization and quantitation of pyridylhydroxybutyl phosphate adducts

Table 1 summarizes the possible numbers of DNA phosphate adduct isomers which could be formed from intermediates produced in the metabolism of NNAL. There can be 10 different combinations of the four nucleobases, and there can be different stereoisomers for each combination due to the chiral centers in the structure. Thus, because of the tetrahedral structure of the phosphate group and the chiral carbinol carbon, there can be four possible isomers of B$_1$p(PHB)$_s$B$_2$ with the same nucleobase combination, and eight isomers with different nucleobase combinations, resulting in a total of 64 different possible B$_1$p(PHB)$_s$B$_2$ adducts. For B$_1$p(PHB)$_b$B$_2$ adducts, an additional chiral center is introduced on the methyl-bearing carbon, so the adducts with the same nucleobase combination can potentially form eight isomers, while adducts with a different nucleobase combination

Table 1. Numbers of possible isomers of pyridylhydroxybutyl phosphate adducts formed from NNAL (see structures of B$_1$p(PHB)$_s$B$_2$ and B$_1$p(PHB)$_b$B$_2$, Figure 1)

Base combination	$[M + H]^+$	$[M + 2H]^{2+}$	Number of possible isomers			Number detected	
			B$_1$p(PHB)$_s$B$_2$	B$_1$p(PHB)$_b$B$_2$	Total	Lung	Liver
A–A	714.2508	357.6293	4	8	12	8	4
C–C	666.2283	333.6181	4	8	12	7	2
G–G	746.2406	373.6242	4	8	12	7	2
T–T	696.2276	348.6177	4	8	12	7	4
A–C	690.2396	345.6237	8	16	24	12	8
A–G	730.2457	365.6268	8	16	24	11	7
A–T	705.2392	353.1235	8	16	24	16	7
C–G	706.2345	353.6212	8	16	24	18	8
C–T	681.2280	341.1179	8	16	24	11	7
G–T	721.2341	361.1210	8	16	24	10	5
Total			64	128	192	107	54

can produce 16 isomers, resulting in a total of 128 different possible $B_1p(PHB)_bB_2$ adducts. Collectively, these straight chain and branched adducts are called $B_1p(PHB)B_2$. Therefore, a total of 192 $B_1p(PHB)B_2$ adducts could be formed from intermediates produced in the metabolism of NNAL. By analyzing the data obtained from both SIM and product ion scans, as described below, we observed at least seven isomers of each combination of $B_1p(PHB)B_2$ phosphate adducts, and a total of 107 and 54 out of 192 possible adducts were detected in rat lung and liver, respectively (Table 1).

The presence of $Cp(PHB)_sC$ and $Tp(PHB)_sT$ in rat tissue DNA was confirmed by comparison of their LC-MS retention times and product ion scan spectra to those of the synthesized standards. Figure 2A shows the chromatogram for standard $Cp(PHB)_sC$ and Figure 2B the corresponding chromatogram of a DNA sample from rat lung upon treatment with NNK in the drinking water for 30 weeks. The first two peaks in Figure 2B match the standard straight chain $Cp(PHB)_sC$ adducts while the remaining peaks arise from the rearranged intermediate **10** and correspond to the branched $Cp(PHB)_bC$ adducts, which were also observed in the reactions of DNA with NNALOAc (see below). Similarly, both $Tp(PHB)_sT$ and $Tp(PHB)_bT$ were observed in the same DNA sample (Figure 2C and D). Detection of 1-(3-pyridyl)-1,3-butanediol (22), which is released from $B_1p(PHB)_bB_2$ adducts upon acid hydrolysis, was used to further confirm the presence of the branched phosphate adducts. To ensure that 1-(3-pyridyl)-1,3-butanediol was from phosphate adducts but not base adducts, the tissue DNA hydrolysate was fractionated by HPLC to separate out PHB base adducts, and the fraction containing only phosphate adducts was subjected to acid hydrolysis (Supplementary Figure 8, available at *Carcinogenesis* Online). Indeed, 1-(3-pyridyl)-1,3-butanediol was detected in the phosphate adduct-containing fraction upon acid hydrolysis, which confirmed the presence of $B_1p(PHB)_bB_2$ adducts in the rat tissue DNA (Supplementary Figure 9, available at *Carcinogenesis* Online).

The structures of the other eight nucleobase combinations were characterized based on the accurate masses of the precursor ions and the corresponding fragment ions. With Ap(PHB)C as an example, the exact mass of its precursor ion of *m/z* 690.2396 was extracted from the SIM scan data upon analysis of lung DNA from a 10 week-treated rat, and 12 peaks were detected (Figure 2E), indicating the presence of at least 12 isomers. The peak shapes and retention times of the major fragment ion, *m/z* 328.0945, and the other major fragment ions of each of the 12 peaks matched the SIM data from the parent ion (Figure 2E and Supplementary Figure 7, available at *Carcinogenesis* Online), further confirming the identity and the structure of the Ap(PHB)C adducts. Since the standards of Ap(PHB)C were not available, discrimination between the straight chain and branched isomers was not possible. The nomenclature of the isomers [Ap(PHB)C-1 to Ap(PHB)C-12] was based on the sequence of their retention times in the chromatogram. The extracted ion chromatograms in rat lung DNA and proposed fragmentation patterns for structural characterization of all the other $B_1p(PHB)B_2$ phosphate adducts are presented in Supplementary Figure 7, available at *Carcinogenesis* Online.

Based on our unexpected observation of more than eight peaks for each combination of different DNA bases, we examined the formation of $B_1p(PHB)B_2$ in CT-DNA treated with NNALOAc, to further confirm their origin. The $B_1p(PHB)B_2$ adducts detected *in vivo* were observed in the *in vitro* NNALOAc-treated CT-DNA sample. As an example, typical extracted precursor and fragment ion (*m/z* 328.0945) chromatograms corresponding to Cp(PHB)C and Tp(PHB)T obtained upon analysis of an NNALOAc-treated CT-DNA sample are presented in Supplementary Figure 10, available at *Carcinogenesis* Online. A total of 97 out of 192 possible $B_1p(PHB)B_2$ adducts were detected (Supplementary Table 1, available at *Carcinogenesis* Online). At least six isomers were observed for each combination of $B_1p(PHB)B_2$ adducts. The three most abundant adduct types formed were Cp(PHB)T, Ap(PHB)T and Ap(PHB)C, which accounted for 24, 21 and 18% of the total $B_1p(PHB)B_2$ adducts, respectively (Supplementary Figure 10, available at *Carcinogenesis* Online).

Using HCD fragmentation, the product ion spectra of both $Cp(PHB)_sC$ and $Tp(PHB)_sT$ generated several major fragment ions (Supplementary Figure 11, available at *Carcinogenesis* Online). Because of the high signal intensity in the spectra of both $Cp(PHB)_sC$ and $Tp(PHB)_sT$, the fragment ion of *m/z* 328.0945 was selected for quantitative analysis, with the transitions of *m/z* 666.2→328.0945 for $Cp(PHB)_sC$, *m/z* 669.2→328.0945 for $[^{15}N_3]Cp(PHB)_sC$, *m/z* 696.2→328.0945 for $Tp(PHB)_sT$, and *m/z* 708.2→328.0945 for $[^{13}C_{10}{}^{15}N_2]Tp(PHB)_sT$. Typical chromatograms obtained upon analysis of $Cp(PHB)_sC$ and $Tp(PHB)_sT$ standards are presented in Figure 2. Only two of the possible four isomers were detected for $Cp(PHB)_sC$ [$Cp(PHB)_sC$-1 and $Cp(PHB)_sC$-2], likely due to insufficient chromatographic resolution of all isomers under our conditions. Similarly, only two peaks were detected for the four possible isomers of $Tp(PHB)_sT$ without baseline separation, and the total area of the two peaks was used for quantitative analysis. By using this method, a limit of detection of 0.03 fmol on-column was obtained for $Cp(PHB)_sC$-1, $Cp(PHB)_sC$-2 and $Tp(PHB)_sT$. The instrument response and the analyte/internal standard ratio were linear in the range of 0.03–15 fmol on-column with typical R^2 of 0.9983, 0.9996 and 0.9998 for $Cp(PHB)_sC$-1, $Cp(PHB)_sC$-2, and $Tp(PHB)_sT$ (Figure 2F–H), respectively. The calibration curves were then used for quantitation of $B_1p(PHB)B_2$ adducts in the rat tissue DNA samples.

$B_1p(PHB)B_2$ phosphate adducts in rat tissue DNA

Three major $B_1p(PHB)B_2$ phosphate adducts were observed in rat liver DNA—Cp(PHB)T, Ap(PHB)C and Tp(PHB)T—which accounted for 21–23, 19–24 and 15–25% of the total $B_1p(PHB)B_2$ phosphate adducts, respectively (Figure 3A). A decrease in adduct levels over the course of the study was observed for all the combinations. For example, the level of Ap(PHB)C decreased from 441 ± 38 fmol/mg DNA at 10 weeks of treatment to 210 ± 77 fmol/mg DNA at 70 weeks of treatment ($P < 0.05$). In the lung, the three most abundant adducts were Cp(PHB)T, Ap(PHB)C and Gp(PHB)T, which accounted for 20–30, 16–19 and 10–17% of the total $B_1p(PHB)B_2$ phosphate adducts, respectively (Figure 3B). However, the formation patterns were different between the two tissues. While the adduct levels of most combinations were maximal at 10 weeks in the liver, the levels of most combinations were the highest at 30 weeks in the lung. For example, the level of Ap(PHB)C in the lung at 30 weeks was 1410 ± 76 fmol/mg DNA, significantly higher than the levels at 10, 50 or 70 weeks ($P < 0.05$).

Different levels of isomers of the same combination of $B_1p(PHB)B_2$ were observed for all 10 combinations in both liver and lung (Figure 3C–E and Supplementary Figures 12 and 13, available at *Carcinogenesis* Online). For example, the level of Gp(PHB)T-1 was significantly higher than the other isomers of Gp(PHB)T in the liver throughout the study (Figure 3C). The formation patterns of each isomer from some combinations were similar. For example, the levels of both $Cp(PHB)_sC$-1 and $Cp(PHB)_sC$-2 in the liver were maximal at 10 weeks and decreased afterwards (Figure 3D). However, the formation patterns of isomers from some other combinations were different. For example, the level of

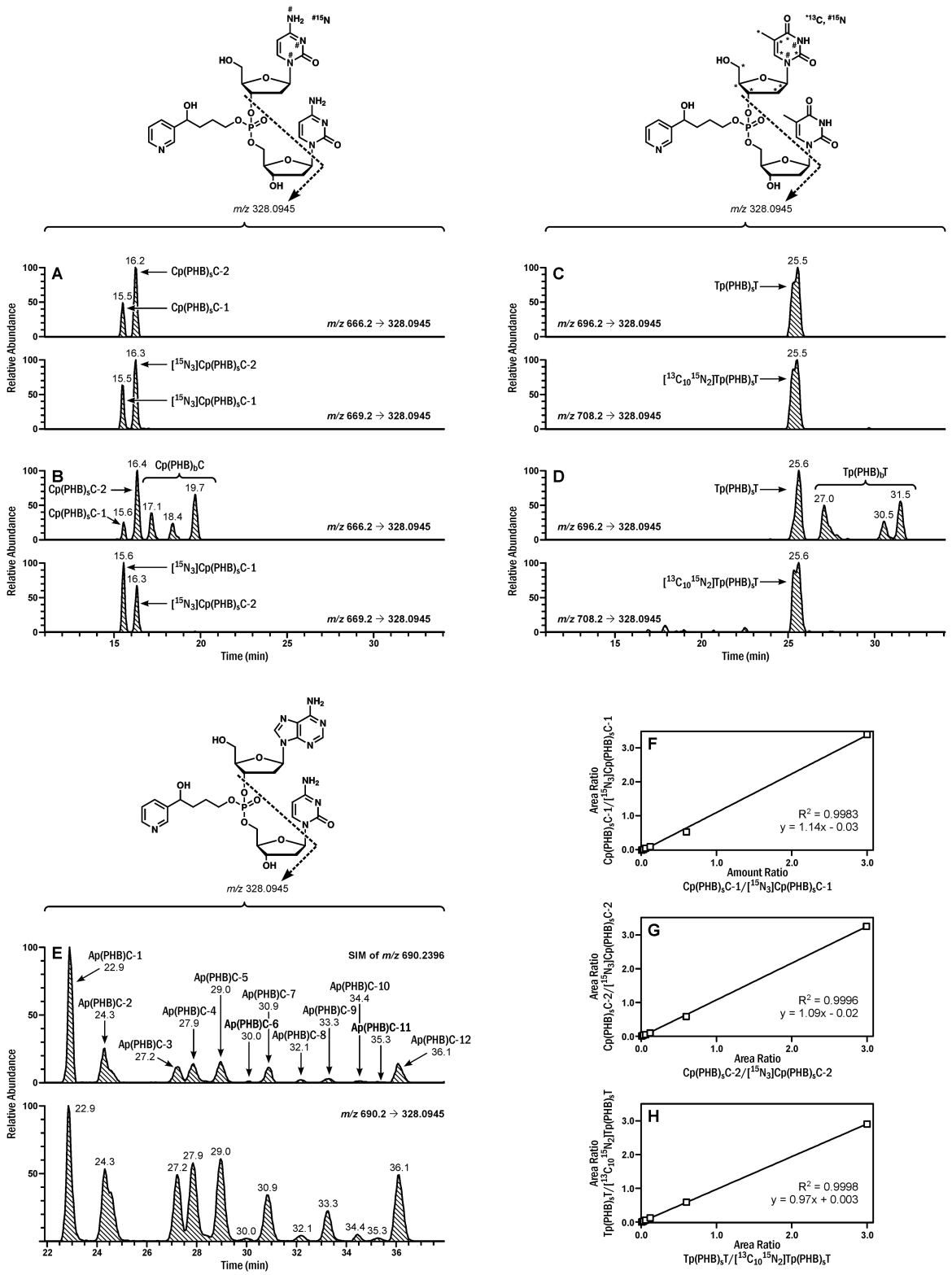

Figure 2. Typical chromatograms obtained upon analysis of (**A**) $Cp(PHB)_sC$ standards, (**B**) Cp(PHB)C in lung DNA of a rat treated with NNK in drinking water (5 ppm) for 30 weeks, (**C**) $Tp(PHB)_sT$ standards, (**D**) Tp(PHB)T in lung DNA of a rat treated with NNK in drinking water (5 ppm) for 30 weeks; (**E**) LC-NSI-HRMS/MS extracted precursor (*m/z* 690.2396, SIM, selected-ion monitoring) and fragment ion (*m/z* 328.0945) chromatograms corresponding to Ap(PHB)C obtained upon analysis of lung DNA of a rat treated with NNK in drinking water (5 ppm) for 10 weeks; Linearity of (**F**) $Cp(PHB)_sC$-1, (**G**) $Cp(PHB)_sC$-2 and (**H**) $Tp(PHB)_sT$ calibration curves. The amount of $Cp(PHB)_sC$ or $Tp(PHB)_sT$ in the calibration curve was increased from 0.03 fmol to 0.06, 0.15, 0.3, 0.6, 3 and 15 fmol, with a constant amount of internal standards (5 fmol).

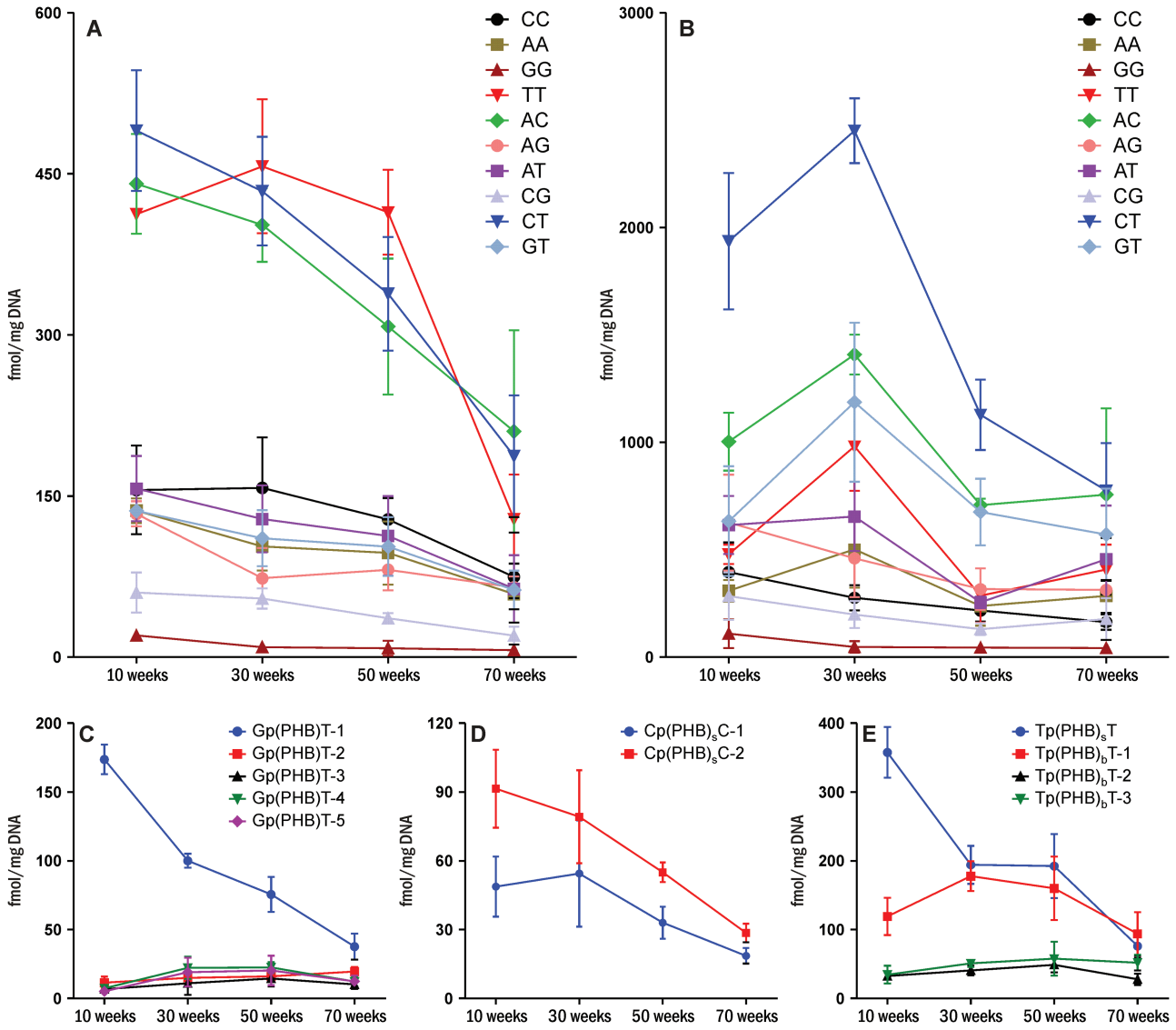

Figure 3. Levels of pyridylhydroxybutyl DNA phosphate adducts in (**A**) liver DNA, (**B**) lung DNA, and levels of each isomer of (**C**) Gp(PHB)T, (**D**) Cp(PHB)C and (**E**) Tp(PHB)T in liver DNA of rats (n = 5) treated with 5 ppm of NNK in drinking water for 10, 30, 50 or 70 weeks. Values are presented as means ± SD.

$Tp(PHB)_s$T-1 in the liver was maximal at 10 weeks and decreased afterwards ($P < 0.05$, Figure 3E), while the levels of $Tp(PHB)_b$T-1 and $Tp(PHB)_b$T-2 reached a peak at 30 and 50 weeks, respectively. The level of $Tp(PHB)_b$T-3 was not significantly changed over the course of the study ($P = 0.14$, Figure 3E).

Comparison of DNA phosphate and base adducts formed by NNK

To determine the relative proportion of $B_1p(PHB)B_2$ adducts to the total known pyridine-containing DNA adducts formed by NNK, the levels of the other three types of DNA adducts [PHB base adducts, POB base adducts and $B_1p(POB)B_2$ adducts], were measured or obtained from our previous studies of rats from the same treatment groups (Table 2) (5,21). The levels of the PHB base adducts—O^2-[4-(3-pyridyl)-4-hydroxybut-1-yl]thymidine (O^2-PHB-dThd) and 7-[4-(3-pyridyl)-4-hydroxybut-1-yl]guanine (7-PHB-Gua)—were measured in rat liver DNA in this study using our previously developed method (24). The total amount of the two major PHB base adducts ranged from 466 to 1050 fmol/mg DNA in liver DNA over the course of the study. The levels of POB base adducts and $B_1p(POB)B_2$ phosphate adducts in the liver and lung were reported previously (5,21). In rat liver, the most abundant type of DNA adducts were POB base adducts, which accounted for 40–44% of the total measured DNA adducts, followed by $B_1p(PHB)B_2$ phosphate adducts (34–40%), PHB base adducts (14–21%) and $B_1p(POB)B_2$ adducts (2–4%) (Figure 4A; Table 2); while in the lung, the most abundant DNA adducts were $B_1p(PHB)B_2$ phosphate adducts, which accounted for 38–55% of the total measured DNA adducts, followed by POB base adducts (32–48%), PHB base adducts (10–13%) and $B_1p(POB)B_2$ phosphate adducts (1–2%) (Figure 4B and Table 2). Methyl-DNA base adducts are also formed by NNK due to α-hydroxylation on its methylene carbon (4,5), and the formation and characterization of methyl-DNA phosphate adducts in NNK-treated rats will be reported separately.

In addition to O^2-PHB-dThd and 7-PHB-Gua, O^6-[4-(3-pyridyl)-4-hydroxybut-1-yl]deoxyguanosine (O^6-PHB-dGuo) was also detected and quantified in NNALOAc-treated CT-DNA. The relative levels of total $B_1p(PHB)B_2$ adducts and total PHB base adducts were comparable to those in the DNA samples from

Table 2. Levels of three major POB base adducts, two major PHB base adducts, total $B_1p(PHB)B_2$ phosphate adducts and total $B_1p(POB)B_2$ phosphate adducts in liver and lung DNA of rats treated with 5 ppm of NNK in drinking water for 10, 30, 50 or 70 weeks

Tissue	Adduct		Adduct level (fmol/mg DNA)			
Liver	POB base[a]		10 weeks	30 weeks	50 weeks	70 weeks
		O^2-POB-dThd	1810 ± 840	2140 ± 26	1530 ± 161	910 ± 6
		7-POB-Gua	501 ± 53	331 ± 36	257 ± 32	230 ± 90
	PHB base					
		O^2-PHB-dThd	390 ± 185	737 ± 186	658 ± 107	272 ± 86
		7-PHB-Gua	335 ± 40	313 ± 79	295 ± 42	194 ± 32
	Total $B_1p(PHB)B_2$ phosphate		2140 ± 131	1930 ± 81	1630 ± 166	878 ± 210
	Total $B_1p(POB)B_2$ phosphate[a]		190 ± 49	134 ± 64	120 ± 36	89 ± 4
Lung	POB base[b]	O^6-POB-dG	34 ± 21	9 ± 9	9 ± 2	4 ± 2
		O^2-POB-dThd	3590 ± 414	4810 ± 193	4410 ± 320	1980 ± 467
		7-POB-Gua	970 ± 148	751 ± 29	688 ± 65	315 ± 75
	PHB base[b]					
		O^2-PHB-dThd	968 ± 28	1370 ± 94	1260 ± 66	807 ± 142
		7-PHB-Gua	235 ± 40	164 ± 44	129 ± 34	62 ± 15
	Total $B_1p(PHB)B_2$ phosphate		6390 ± 457	8160 ± 654	4000 ± 291	3950 ± 223
	Total $B_1p(POB)B_2$ phosphate[a]		475 ± 95	417 ± 43	346 ± 41	218 ± 15

Values are presented as means ± SD (n = 3 or 5).
[a]The data of total $B_1p(POB)B_2$ phosphate adduct levels in both tissues, and POB base adduct levels in rat liver are from Ma *et al.* (21).
[b]The data of POB and PHB base adduct levels in rat lung are from Balbo *et al.* (5).

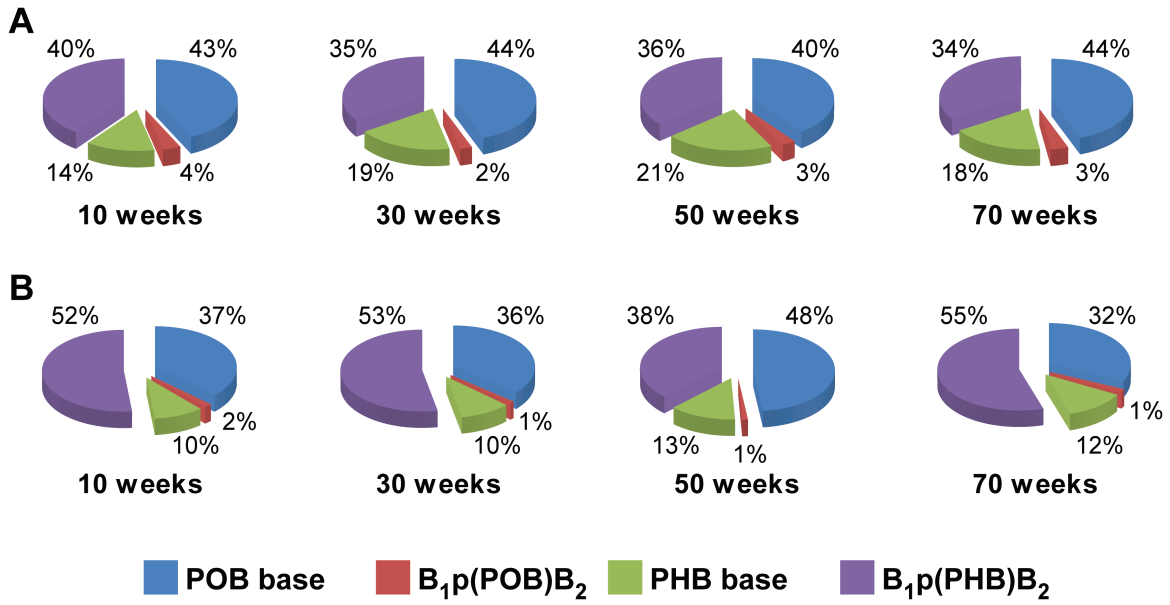

Figure 4. Relative levels of DNA phosphate and base adducts in (**A**) liver and (**B**) lung DNA of rats treated with 5 ppm of NNK in drinking water for 10, 30, 50 or 70 weeks.

treated rats, accounting for 48 and 52% of the total measured DNA adducts, respectively (Supplementary Figure 10, available at *Carcinogenesis* Online).

Discussion

The results of this study were unexpected with respect to both the extent and diversity of DNA phosphate adducts—$B_1p(PHB)B_2$—formed in the NNAL pathway of NNK metabolism. Thus, our previous study of $B_1p(POB)B_2$ adducts formed in NNK metabolism demonstrated that they comprised a relatively small percentage of total adduct formation (Figure 4). In contrast, the present results show that $B_1p(PHB)B_2$ adducts represent a sizable slice of the NNK-DNA adduct pie in rat liver and lung (Figure 4). Notably, our LC-NSI-HRMS/MS method revealed a surprising variety of NNAL-derived DNA phosphate adducts, explainable by the recognition that rearrangement of diazonium ion **9** to carbocation **10** is a substantial *in vivo* pathway of NNAL-DNA adduct formation. Thus, we demonstrate an unprecedented diversity of structurally unique DNA adducts formed from a single

carcinogen—NNK. Taken together with our previous study in which we characterized 30 $B_1p(POB)B_2$ adducts, we have now identified 137 novel and structurally distinct DNA-phosphate adducts in tissues of rats treated with NNK, far greater than reported to date from any other carcinogen.

Most DNA adduct studies have focused on the interaction of chemicals with DNA nucleobases rather than the inter-nucleotide phosphate groups. Studies of DNA phosphate adducts have demonstrated however that they have longer half-lives than their corresponding base adducts in animals treated with alkylating agents (25–28). For example, after administration of a single dose of ethylnitrosourea to mice, the half-lives of ethyl phosphate adducts in the major tissues were 10–15 weeks, compared to the half-lives of 30–220 h of the corresponding O^6-ethylguanine base adduct (28). While the levels of most DNA base adducts decreased over time upon chronic treatment of rats with NNK (5), our previous study demonstrated that the levels of some NNK-derived $B_1p(POB)B_2$ adducts were persistently high in the same rats over the 70 weeks of treatment (21). Consistent with those observations, some of the $B_1p(PHB)B_2$ phosphate adducts in the current study demonstrated persistence in rats over the 70 weeks of treatment. These findings indicate that these DNA phosphate adducts could potentially be used as biomarkers for chronic exposure to tobacco-specific carcinogens in humans. Exploring this approach would most likely involve focusing on a particular isomer such as $Tp(PHB)_bT$-3 in lung. The first step would be further characterization of the selected isomer. This could be accomplished by synthesis of the appropriate diastereoisomeric precursors related to 1-(3-pyridyl)-1,3-butanediol, then reaction of these with the selected dinucleotide phosphate followed by isolation and characterization. With specific standards in hand, analytical methods could be developed for quantitation in cellular DNA from human lung or oral tissue. Based on the high sensitivity and selectivity of LC-NSI-HRMS/MS analysis, this research direction appears feasible.

As noted above, $B_1p(PHB)B_2$ phosphate adducts are formed to a greater extent than $B_1p(POB)B_2$ phosphate adducts in rats treated with NNK. In rat liver, the levels of $B_1p(PHB)B_2$ phosphate adducts (878–2140 fmol/mg DNA) were significantly higher than $B_1p(POB)B_2$ phosphate adducts (89–190 fmol/mg DNA). Similarly, in the lung, the levels of $B_1p(PHB)B_2$ phosphate adducts were 3950–8160 fmol/mg DNA, compared to 218–475 fmol/mg DNA of $B_1p(POB)B_2$ phosphate adducts. These differences were possibly due to the pharmacokinetic properties of NNK. When NNK is administered to rats, it is rapidly converted to NNAL. Although NNAL and NNK are in equilibrium, the equilibrium is strongly shifted toward NNAL in rats (4,29). Moreover, the half-life of NNAL in rats is 298 min, while that of NNK is only 25 min (30). Therefore, NNAL predominates over NNK in the rat circulation system (30,31). Since $B_1p(PHB)B_2$ phosphate adducts were formed from NNAL, while $B_1p(POB)B_2$ adducts were from NNK, this is one explanation for the higher levels of $B_1p(PHB)B_2$ than $B_1p(POB)B_2$ adducts. Indeed, the relative amount of total pyridine-containing DNA adducts from NNAL [$B_1p(PHB)B_2$ plus PHB-base, 51–67%] was higher than that from NNK [$B_1p(POB)B_2$ plus POB-base, 33–49%] in the lung. Similarly, slightly higher levels of NNAL-derived adducts (52–57%) than NNK-derived adducts (43–48%) were observed in the liver. Interestingly, POB base adducts were more abundant than $B_1p(POB)B_2$ phosphate adducts, while PHB base adducts were less abundant than $B_1p(PHB)B_2$ phosphate adducts. This suggests that NNK-derived base and phosphate adducts are either formed or repaired in a different manner than NNAL-derived base and phosphate adducts. However, the repair mechanism of the NNK/NNAL-derived DNA phosphate adducts is still unclear, and further studies are warranted.

The biological significance of the newly characterized NNK/NNAL-derived $B_1p(PHB)B_2$ phosphate adducts is unclear. Studies on other modifications of phosphate groups in DNA suggest some potential effects, including inhibiting DNA metabolic enzymes (25,32,33), affecting DNA helicases (34–36) and interfering with the binding of DNA to other macromolecules (37). Similar effects could be caused by the NNK-derived phosphate adducts, potentially leading to detrimental biological consequences; therefore, further studies of their effects on DNA repair processes and other biological effects are needed.

In summary, we applied our highly sensitive and selective LC-NSI-HRMS/MS methodology to characterize and quantify 54 and 107 previously unknown pyridylhydroxybutyl DNA phosphate adducts formed in liver and lung, respectively, of F-344 rats as the result of exposure to the tobacco-specific carcinogen NNK. These adducts are formed via NNK metabolism to NNAL and subsequent bioactivation of NNAL. Levels of some of these newly identified adducts in lung and liver of NNK-treated rats were persistent over the 70 weeks of treatment. These novel adducts could potentially serve as biomarkers of NNK exposure and carcinogenesis in humans.

Supplementary material

Supplementary data are available at *Carcinogenesis* online.

Funding

This work was supported by National Cancer Institute (CA-81301). Mass spectrometry was carried out in the Analytical Biochemistry Shared Resource of the Masonic Cancer Center, supported in part by Cancer Center Support Grant from National Cancer Institute (CA-77598). Salary support for P.W.V. was provided by National Cancer Institute (CA-211256).

Acknowledgements

We thank Xun Ming for his help with the mass spectrometry analysis, and Dr. Silvia Balbo for providing rat lung DNA samples. We thank Christopher Seiler in Department of Medicinal Chemistry, University of Minnesota for useful discussions on the synthesis of $[^{13}C_{10}{}^{15}N_2]2'$-TpT. We also thank Robert Carlson for editorial assistance.

Conflict of Interest Statement: None declared.

References

1. International Agency for Research on Cancer. (2007) Smokeless tobacco and tobacco-specific nitrosamines. IARC monographs on the evaluation of carcinogenic risks to humans. Vol. 89. International Agency for Research on Cancer: Lyon, France.
2. Appleton, S. *et al.* (2013) TSNA levels in machine-generated mainstream cigarette smoke: 35 years of data. Regul. Toxicol. Pharmacol., 66, 197–207.
3. Hecht, S.S. (2014) It is time to regulate carcinogenic tobacco-specific nitrosamines in cigarette tobacco. Cancer Prev. Res. (Phila)., 7, 639–647.
4. Hecht, S.S. (1998) Biochemistry, biology, and carcinogenicity of tobacco-specific N-nitrosamines. Chem. Res. Toxicol., 11, 559–603.
5. Balbo, S. *et al.* (2014) Carcinogenicity and DNA adduct formation of 4-(methylnitrosamino)-1-(3-pyridyl)-1-butanone and enantiomers of its metabolite 4-(methylnitrosamino)-1-(3-pyridyl)-1-butanol in F-344 rats. Carcinogenesis, 35, 2798–2806.
6. Hecht, S.S. *et al.* (2016) Exposure and metabolic activation biomarkers of carcinogenic tobacco-specific nitrosamines. Acc. Chem. Res., 49, 106–114.

7. Appleton, S. *et al.* (2014) TSNA exposure from cigarette smoking: 18 years of urinary NNAL excretion data. Regul. Toxicol. Pharmacol., 68, 269–274.
8. Hecht, S.S. *et al.* (2002) Quantitation of metabolites of 4-(methylnitrosamino)-1-(3-pyridyl)-1-butanone after cessation of smokeless tobacco use. Cancer Res., 62, 129–134.
9. Hecht, S.S. *et al.* (2007) Similar exposure to a tobacco-specific carcinogen in smokeless tobacco users and cigarette smokers. Cancer Epidemiol. Biomarkers Prev., 16, 1567–1572.
10. Kresty, L.A. *et al.* (1996) Metabolites of a tobacco-specific nitrosamine, 4-(methylnitrosamino)-1-(3-pyridyl)-1-butanone (NNK), in the urine of smokeless tobacco users: relationship between urinary biomarkers and oral leukoplakia. Cancer Epidemiol. Biomarkers Prev., 5, 521–525.
11. Stepanov, I. *et al.* (2005) Tobacco-specific nitrosamines and their pyridine-N-glucuronides in the urine of smokers and smokeless tobacco users. Cancer Epidemiol. Biomarkers Prev., 14, 885–891.
12. Burns, D.M. *et al.* (2011) Do changes in cigarette design influence the rise in adenocarcinoma of the lung? Cancer Causes Control, 22, 13–22.
13. Andreotti, G. *et al.* (2017) Tobacco use and cancer risk in the Agricultural Health Study. Cancer Epidemiol. Biomarkers Prev., 26, 769–778.
14. Ronai, Z.A. *et al.* (1993) G to A transitions and G to T transversions in codon 12 of the Ki-ras oncogene isolated from mouse lung tumors induced by 4-(methylnitrosamino)-1-(3-pyridyl)-1-butanone (NNK) and related DNA methylating and pyridyloxobutylating agents. Carcinogenesis, 14, 2419–2422.
15. Jasti, V.P. *et al.* (2011) Tobacco-specific nitrosamine-derived O2-alkylthymidines are potent mutagenic lesions in SOS-induced *Escherichia coli*. Chem. Res. Toxicol., 24, 1833–1835.
16. Jalas, J.R. *et al.* (2005) Cytochrome P450 enzymes as catalysts of metabolism of 4-(methylnitrosamino)-1-(3-pyridyl)-1-butanone, a tobacco specific carcinogen. Chem. Res. Toxicol., 18, 95–110.
17. Wang, M. *et al.* (2003) Identification of adducts formed by pyridyloxobutylation of deoxyguanosine and DNA by 4-(acetoxymethylnitrosamino)-1-(3-pyridyl)-1-butanone, a chemically activated form of tobacco specific carcinogens. Chem. Res. Toxicol., 16, 616–626.
18. Hecht, S.S. *et al.* (2004) Identification of O^2-substituted pyrimidine adducts formed in reactions of 4-(acetoxymethylnitrosamino)-1-(3-pyridyl)-1-butanone and 4-(acetoxymethylnitros- amino)-1-(3-pyridyl)-1-butanol with DNA. Chem. Res. Toxicol., 17, 588–597.
19. Sturla, S.J. *et al.* (2005) Mass spectrometric analysis of relative levels of pyridyloxobutylation adducts formed in the reaction of DNA with a chemically activated form of the tobacco-specific carcinogen 4-(methylnitrosamino)-1-(3-pyridyl)-1-butanone. Chem. Res. Toxicol., 18, 1048–1055.
20. Lao, Y. *et al.* (2006) Quantitation of pyridyloxobutyl DNA adducts of tobacco-specific nitrosamines in rat tissue DNA by high-performance liquid chromatography-electrospray ionization-tandem mass spectrometry. Chem. Res. Toxicol., 19, 674–682.
21. Ma, B. *et al.* (2015) Comprehensive high-resolution mass spectrometric analysis of DNA phosphate adducts formed by the tobacco-specific lung carcinogen 4-(methylnitrosamino)-1-(3-pyridyl)-1-butanone. Chem. Res. Toxicol., 28, 2151–2159.
22. Spratt, T.E. *et al.* (1990) Solvolysis of model compounds for alpha-hydroxylation of N'-nitrosonornicotine and 4-(methylnitrosamino)-1-(3-pyridyl)-1-butanone: evidence for a cyclic oxonium ion intermediate in the alkylation of nucleophiles. Chem. Res. Toxicol., 3, 350–356.
23. Upadhyaya, P. *et al.* (2008) Quantitation of pyridylhydroxybutyl-DNA adducts in liver and lung of F-344 rats treated with 4-(methylnitrosamino)-1-(3-pyridyl)-1-butanone and enantiomers of its metabolite 4-(methylnitrosamino)-1-(3-pyridyl)-1-butanol. Chem. Res. Toxicol., 21, 1468–1476.
24. Zhang, S. *et al.* (2009) Analysis of pyridyloxobutyl and pyridylhydroxybutyl DNA adducts in extrahepatic tissues of F344 rats treated chronically with 4-(methylnitrosamino)-1-(3-pyridyl)-1-butanone and enantiomers of 4-(methylnitrosamino)-1-(3-pyridyl)-1-butanol. Chem. Res. Toxicol., 22, 926–936.
25. Jones, G.D. *et al.* (2010) Phosphotriester adducts (PTEs): DNA's overlooked lesion. Mutagenesis, 25, 3–16.
26. Singer, B. (1985) *In vivo* formation and persistence of modified nucleosides resulting from alkylating agents. Environ. Health Perspect., 62, 41–48.
27. Den Engelse, L. *et al.* (1987) O^2- and O^4-ethylthymine and the ethylphosphotriester dTp(Et)dT are highly persistent DNA modifications in slowly dividing tissues of the ethylnitrosourea-treated rat. Carcinogenesis, 8, 751–757.
28. Shooter, K.V. *et al.* (1977) The stability of methyl and ethyl phosphotriesters in DNA *in vivo*. Chem. Biol. Interact., 19, 353–361.
29. Upadhyaya, P. *et al.* (2000) Formation and metabolism of 4-(methylnitrosamino)-1-(3-pyridyl)-1-butanol enantiomers *in vitro* in mouse, rat and human tissues. Carcinogenesis, 21, 1233–1238.
30. Adams, J.D. *et al.* (1985) On the pharmacokinetics of tobacco-specific N-nitrosamines in Fischer rats. Carcinogenesis, 6, 509–511.
31. Adams, J.D. *et al.* (1985) Pharmacokinetics of N'-nitrosonornicotine and 4-(methylnitrosamino)-1-(3-pyridyl)-1-butanone in laboratory animals. Cancer Lett., 28, 195–201.
32. Yashiki, T. *et al.* (1992) Sequence specific block of in vitro DNA synthesis with isopropyl phosphotriesters in template oligodeoxyribonucleotides. Nucleic Acids Symp. Ser., 27, 197–198.
33. Miller, P.S. *et al.* (1982) Synthesis and template properties of an ethyl phosphotriester modified decadeoxyribonucleotide. Biochemistry, 21, 5468–5474.
34. Eoff, R.L. *et al.* (2005) Chemically modified DNA substrates implicate the importance of electrostatic interactions for DNA unwinding by Dda helicase. Biochemistry, 44, 666–674.
35. Suhasini, A.N. *et al.* (2012) DNA repair and replication fork helicases are differentially affected by alkyl phosphotriester lesion. J. Biol. Chem., 287, 19188–19198.
36. Khan, I. *et al.* (2015) Close encounters for the first time: helicase interactions with DNA damage. DNA Repair (Amst)., 33, 43–59.
37. Makishi, S. *et al.* (2014) Modulation of binding properties of amphiphilic DNA containing multiple dodecyl phosphotriester linkages to lipid bilayer membrane. Bioorg. Med. Chem. Lett., 24, 3578–3581.